Nanoscale Advances

ROYAL SOCIETY OF CHEMISTRY

PAPER

View Article Online
View Journal | View Issue

Cite this: *Nanoscale Adv.*, 2023, **5**, 4911

Fast synthesis of [1,2,3]-triazole derivatives on a Fe/Cu-embedded nano-catalytic substrate†

Nima Khaleghi, Zahrasadat Mojtabapour,‡ Zahra Rashvandi, Adibeh Mohammadi, Mohadeseh Forouzandeh-Malati, Fatemeh Ganjali, Simindokht Zarei-Shokat, Amir Kashtiaray, Reza Taheri-Ledari * and Ali Maleki *

Received 14th May 2023
Accepted 6th August 2023

DOI: 10.1039/d3na00326d

rsc.li/nanoscale-advances

Triazoles are biologically important compounds that play a crucial role in biomedical applications. In this study, we present an innovative and eco-friendly nanocatalyst system for synthesizing compounds *via* the click reaction. The system is composed of Arabic gum (AG), iron oxide magnetic nanoparticles (Fe_3O_4 MNPs), (3-chloropropyl) trimethoxysilane (CPTMS), 2-aminopyridine (AP), and Cu(I) ions. Using AP as an anchor for Cu(I) ions and Fe_3O_4 MNPs allows facile separation using an external magnet. The hydrophilic nature of the Fe_3O_4@AG/AP-Cu(I) nanocomposite makes it highly efficient in water as a green solvent. The highest reaction efficiency (95.0%) was achieved in H_2O solvent with 50.0 mg of nanocatalyst for 60 min at room temperature. The reaction yield remained consistent for six runs, demonstrating the stability and effectiveness of the catalyst.

1. Introduction

Heterocycles are a large group of organic compounds with high biological properties, including anticancer, antimicrobial, anti-Alzheimer, anti-obesity, anti-diabetic, antihistaminic, anticonvulsant, antiviral, and antiparasitic properties, and are widely used in medicinal compounds.[1] In recent decades, research based on triazole derivatives as medicinal compounds has received much attention, and impressive results have been obtained.[2,3] Triazole compounds contain a five-membered aromatic azole ring with three nitrogen atoms, which can connect to various enzymes and receptors in the biological system through non-covalent bonds and show excellent biological activities.[4] One of the methods for developing triazole products is azide-alkyne Huisgen cycloaddition which occurs between an azide and a terminal or internal alkyne to give a 1,2,3-triazole and named the click reaction.[5] The Azide-alkyne Huisgen cycloaddition reaction, which produces covalently linked molecules *via* a 1,2,3-triazole, is among the superior transformations in synthetic organic chemistry.[6,7]

Click reactions are gaining tremendous attention because they allow chemists to connect two building blocks easily.[8] The distinctive features of thermodynamically controlled copper-catalyzed azide-alkyne cycloaddition, such as facile and moderate reaction conditions, compatibility with a wide range of different functional groups and various solvents, and wide pH range tolerance, introduce this reaction as a powerful method for biologically pertinent molecule synthesis and modification of organic scaffolds.[9] Nevertheless, high reaction temperature and lack of regioselectivity are the main disadvantages of this reaction.[10] Using metal ions as catalysts is a powerful method to accelerate many organic reactions.[11] Studies show that copper metal has been used as a catalyst in the click reaction in several forms, such as metal salt,[12] copper nanoparticles (NPs),[13] copper stabilized on polymer substrates,[14] $CuSO_4$-ascorbate systems,[15] and nanostructured copper oxide.[16] According to reports, heterogeneous catalytic systems have attracted much attention in both micro and nanoscales due to the high surface area for chemical reactions between the reactants and the catalytic substrate.[17]

One of the essential features in constructing heterogeneous catalysts is their easy separation from the reaction flask.[18] In this regard, heterogeneous catalytic systems based on MNPs are widely used due to their easy separation by using an external magnet.[19–36] Over the past few decades, MNPs with a unique size and structure have garnered significant attention due to their distinct physical and chemical properties.[37,38] A multitude of strategies have been developed to synthesize a variety of magnetic nanomaterials, including iron, cobalt, nickel, alloys, iron oxide, metal ferrite, and more.[39–41] Among all magnetic materials, magnetite (Fe_3O_4) is the most important and widely utilized in numerous fields.[42] When engineered into well-defined nanoscale structures, Fe_3O_4 exhibits vast potential for

Catalysts and Organic Synthesis Research Laboratory, Department of Chemistry, Iran University of Science and Technology, Tehran 16846-13114, Iran. E-mail: Rezataheri13661206@gmail.com; R_taheri94@alumni.iust.ac.ir; maleki@iust.ac.ir; Fax: +98 2173021584; Tel: +98 21 77240640-50

† Electronic supplementary information (ESI) available: Supplementary information such as ^{1}HNMR and ^{13}C-NMR spectra of the synthetic products, can be acquired in the online version of this article on the publisher's website. See DOI: https://doi.org/10.1039/d3na00326d

‡ Co-first author.

practical applications in various domains, such as biomolecular separation,[43] chemical sensing,[44] energy storage,[45] catalysis,[46–51] absorption,[52,53] biomedicine/biotechnology,[54–61] and environmental remediation. Fe_3O_4 MNPs can be synthesized using various methods, such as coprecipitation of Fe^{2+} and Fe^{3+}, thermal decomposition, microemulsion, and hydrothermal/solvothermal techniques. Of all the methods mentioned, coprecipitation is the favored option for most researchers due to its ability to be conducted under mild conditions using water as a solvent.[62–65] Due to the high importance of the environment and green chemistry, researchers are looking to make catalysts based on biodegradable and environmentally friendly materials. Accordingly, heterogeneous catalytic systems are modified by different components such as natural polymers, minerals, and biological structures so that more catalytic sites are available.[25,66–70]

AG has a natural origin from wild trees primarily found in Somalia.[71,72] Using natural polymer (AG) is a direct approach to successfully synthesize the aqueous phase of various metal NPs.[73,74] This polymer is widely used as a stabilizer, reducing agent, emulsifying agent, and additive in various NP syntheses.[75–78] The functional hydroxyl groups in the structure of this natural polymer can make a physicochemical hydrogen bond with hydroxyl groups on the surface of MNPs.[79] Other hydroxyl groups not involved in hydrogen bonds can be functionalized by covalent bonds with various linkers.[80] From a green and sustainable chemistry perspective, a recent surge of interest has been in designing efficient and cost-effective chemical processes that utilize heterogeneous catalysts to synthesize fine chemicals and pharmaceutical products through multicomponent reactions (MCRs).[81–83] However, the limited catalytic activity of these catalysts remains a significant challenge. Minimizing the particles' size in the heterogeneous catalyst is crucial to overcome this issue.[84,85] Nanostructured catalysts, which lie at the interface of homogeneous and heterogeneous catalysis, are known as "quasi-homogeneous" or "soluble heterogeneous" catalysts due to their nanoscale nature and high surface area.[86,87]

Nonetheless, conventional separation techniques such as filtration and centrifugation become problematic for suspensions containing particles smaller than 100 nm, making it difficult to separate the catalyst.[88,89] Today, magnetic nanocatalysts are widely used to develop sustainable and green processes due to easy separation, low energy loss, and economic efficiency.[90,91] Fe_3O_4 MNPs have gained prominence due to their unique properties, including easy preparation from low-cost precursors, high surface area, low toxicity, excellent reusability, and biocompatibility.[92] Usually, these NPs are protected by surface functionalization with biological coatings to prevent oxidation and self-assembly and increase stability.[93,94]

In this work, a novel magnetic nanocatalyst is designed based on AG as a natural polymer with low toxicity. First, Fe_3O_4 MNPs were selected as a central core of the nanocatalyst to prepare a magnetic nanocatalyst with easy separation.[95] AG was chosen as the primary cover. The MNPs were incorporated into the AG matrix polymer to improve stability and prevent accumulation. Also, the dispersibility of the nanocomposite can be increased due to the presence of hydrophilic functional groups such as hydroxyl (–OH) and carbonyl (–COOH) groups in the AG structure.[96] For this purpose, Fe_3O_4 MNPs were synthesized in a flask reaction and fixed *in situ* inside the matrix polymer.[97] Following this, the Fe_3O_4@AG nanocomposite surface was modified by CPTMS so that the anchor molecules (AP) could be attached to it. CPTMS was added to the Fe_3O_4@AG solution in this stage and kept under reflux treatment. The AP molecule with a unique dual nucleophilic structure was selected as an anchor to place Cu(I) ions by coordination bonds.[98] Also, this stage was performed by adding AP and triethylamine to the Fe_3O_4@AG@CPTMS solution under reflux conditions. Finally, the Cu(I) ion chelated with nitrogen atoms of the AP compound to act as the active sites for the click reaction. Fourier-transform infrared spectroscopy (FTIR), X-ray diffraction analysis (XRD), energy dispersive X-ray (EDX) spectroscopy, thermogravimetric analysis (TGA), vibrating-sample magnetometry (VSM), and field emission scanning electron microscopy (FESEM) were performed to characterize the Fe_3O_4@AG/AP-Cu(I) nanocomposite and all of them proved its successful synthesis. The synthesis process of the [1,2,3]-triazole derivatives was evaluated in the presence of the Fe_3O_4@AG/AP-Cu(I) nanocatalyst. The highest efficiency (95%) was obtained with optimization parameters such as 50.0 mg (catalyst dosage), 60 min (time reaction), H_2O (solvent), and room temperature. The novel and environmentally friendly nanocatalyst prepared by our research group could be an effective nanocatalyst for synthesizing triazole derivatives. This nanocatalyst's turnover number (TON) and turnover frequency (TOF) values were calculated to be 48.66 and 0.0135, respectively. The novel and environmentally friendly nanocatalyst our research group prepared could be an effective nanocatalyst for synthesizing [1,2,3]-triazole derivatives.

2. Experimental

2.1. Materials and equipment

All the chemical materials, solvents, and reagents were purchased from Sigma-Aldrich and Merck companies. The FTIR analysis was performed by using a Shimadzu FTIR-8400S spectrometer *via* the KBr pellet method. The XRD analysis was performed with a DRON-8 X-ray diffractometer. The EDX spectrum was obtained by using a VEGA-TESCAN-XMU. Also, TGA, inductively coupled plasma optical emission spectroscopy (ICP-OES), and vibrating-sample magnetometry (VSM) were performed by using a Bahr-STA 504 instrument under an argon atmosphere, Varian VIST-MPX with an axial torch, and LBKFB model-magnetic Kashan Kavir (5000 Oe) instrument, respectively.

2.2. Preparation of Fe_3O_4@AG nanopowder

0.64 g of iron(II) and 1.20 g of iron(III) chloride salts were initially dissolved in 10.0 mL of deionized water at an ambient temperature. Afterward, 0.60 g of AG powder was poured and dissolved in the reaction flask. In the next stage, iron ions were precipitated through the co-deposition method, and the formed Fe_3O_4 MNPs were composed of the AG polymer. Finally, the *in situ* method provides a better composition, and immobilization

of the dark Fe_3O_4 MNPs was carried out by using an ammonia solution to increase the pH value to 12.[25]

2.3. Preparation of the Fe_3O_4@AG@CPTMS magnetic nanocomposite

Fe_3O_4@AG (1.0 g) was poured into a round bottom flask containing 20.0 mL dry toluene. First, the obtained mixture was sonicated for 20 min. Next, MNP modification with 3-chloropropyltrimethoxysilane (CPTMS) was accomplished by adding 3.0 mL of CPTMS (16.45 mmol) into the mixture under stirring and reflux in toluene (110 °C) for 24 h, under a N_2 atmosphere. Then, the resultant product was rinsed with absolute ethanol to remove unattached substrates and eventually dried at 100 °C for 12 h.[79]

2.4. Preparation of the Fe_3O_4@AG/AP magnetic nanocomposite

The prepared Fe_3O_4@AG@CPTMS was sonicated for 30 min. Then, 0.4 g AP and 2.0 mL triethylamine were added to a round bottom flask containing 40.0 mL ethanol, and refluxed for 24 h at 70 °C under an N_2 atmosphere to prepare the Fe_3O_4@AG/AP magnetic nanocomposite.

2.5. Preparation of the Fe_3O_4@AG/AP-Cu(I) magnetic nanocomposite

Finally, the catalyst was synthesized by reacting Fe_3O_4@AG/AP with 0.8 g copper(I) chloride. The Cu particles in the prepared Fe_3O_4@AG/AP-Cu(I) act as the active sites for the one-pot synthesis of 1,2,3 triazole derivatives.[99]

2.6. General process of the synthesis of triazole derivatives (4a–q) in the presence of Fe_3O_4@AG/AP-Cu(I)

For the synthesis of triazole derivatives, 1.0 mmol, 1.1 mmol, and 1.0 mmol of each reactant, such as alkyne, sodium azide, and 2-chloro-*N*-phenyl-acetamide, respectively, were mixed in the presence of distilled water (2.0 mL), and 50.0 mg of the prepared nanocatalyst was added to it. The solution mixture was stirred for an appropriate time at room temperature. Next, the nanocatalyst was separated magnetically from the reaction flask. Finally, the product was isolated by filtration and washed several times with ethanol, and the recrystallization process was performed to obtain the pure product.

3. Results and discussion

3.1. Preparation of the Fe_3O_4@AG/AP-Cu(I) magnetic nanocomposite

Our primary objective in this research was to uphold the tenets of green chemistry while enhancing the catalyst's efficacy in synthesizing essential biological compounds like triazoles. To this end, a novel catalyst was developed using a natural polymer and copper ions. This innovation offers numerous benefits, such as being cost-effective and having low toxicity. Our findings demonstrate that this groundbreaking catalyst is exceptionally proficient in synthesizing triazole compounds through click reactions, achieving an unparalleled efficiency rate of 95.0% compared to other catalysts. This high efficiency was achieved only by applying 0.05 g of adsorbent dose.

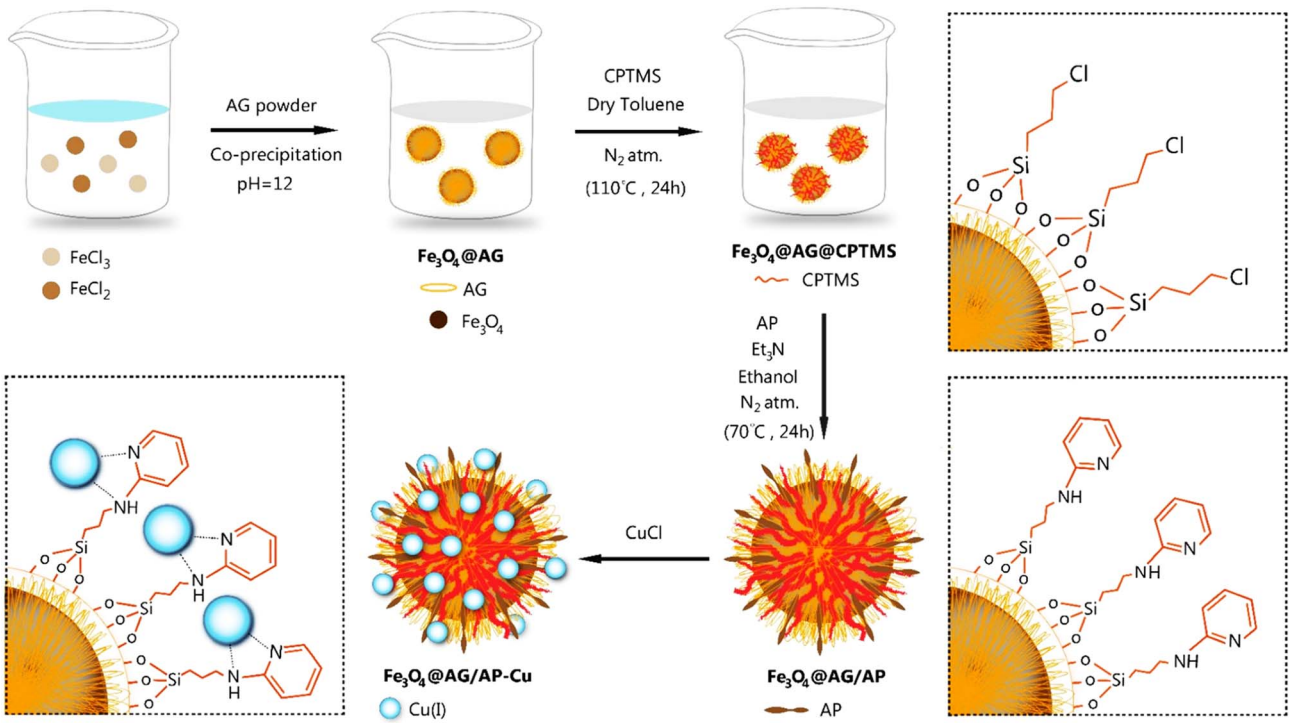

Scheme 1 The preparation process of the Fe_3O_4@AG/AP-Cu(I) magnetic nanocomposite.

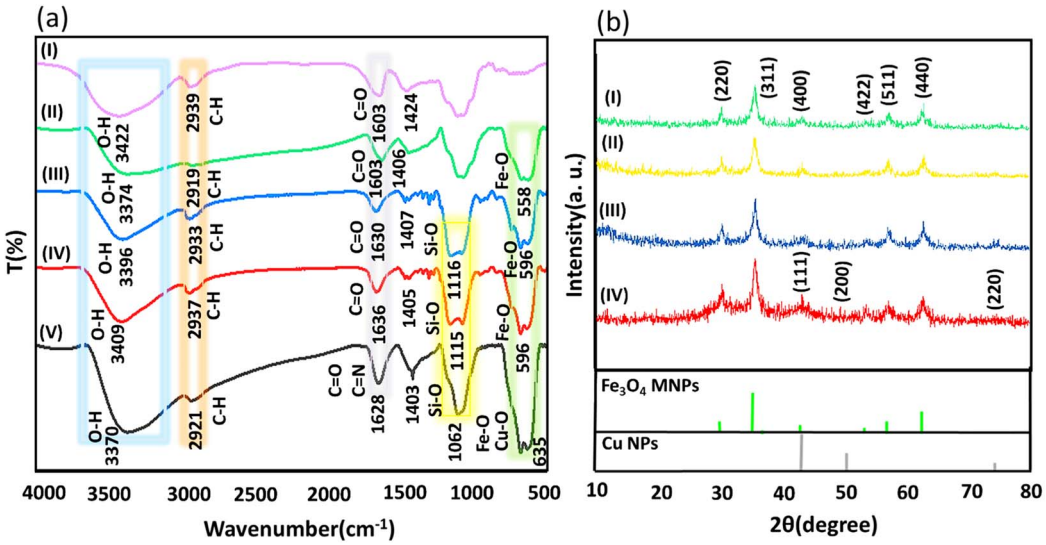

Fig. 1 FTIR spectra of AG (I), Fe_3O_4@AG (II), Fe_3O_4@AG@CPTMS (III), Fe_3O_4@AG/AP (IV), and Fe_3O_4@AG/AP-Cu(I) (V) (a) and XRD patterns of Fe_3O_4@AG (I), Fe_3O_4@AG@CPTMS (II), Fe_3O_4@AG/AP (III), and Fe_3O_4@AG/AP-Cu(I) (IV) nanocomposites (b).

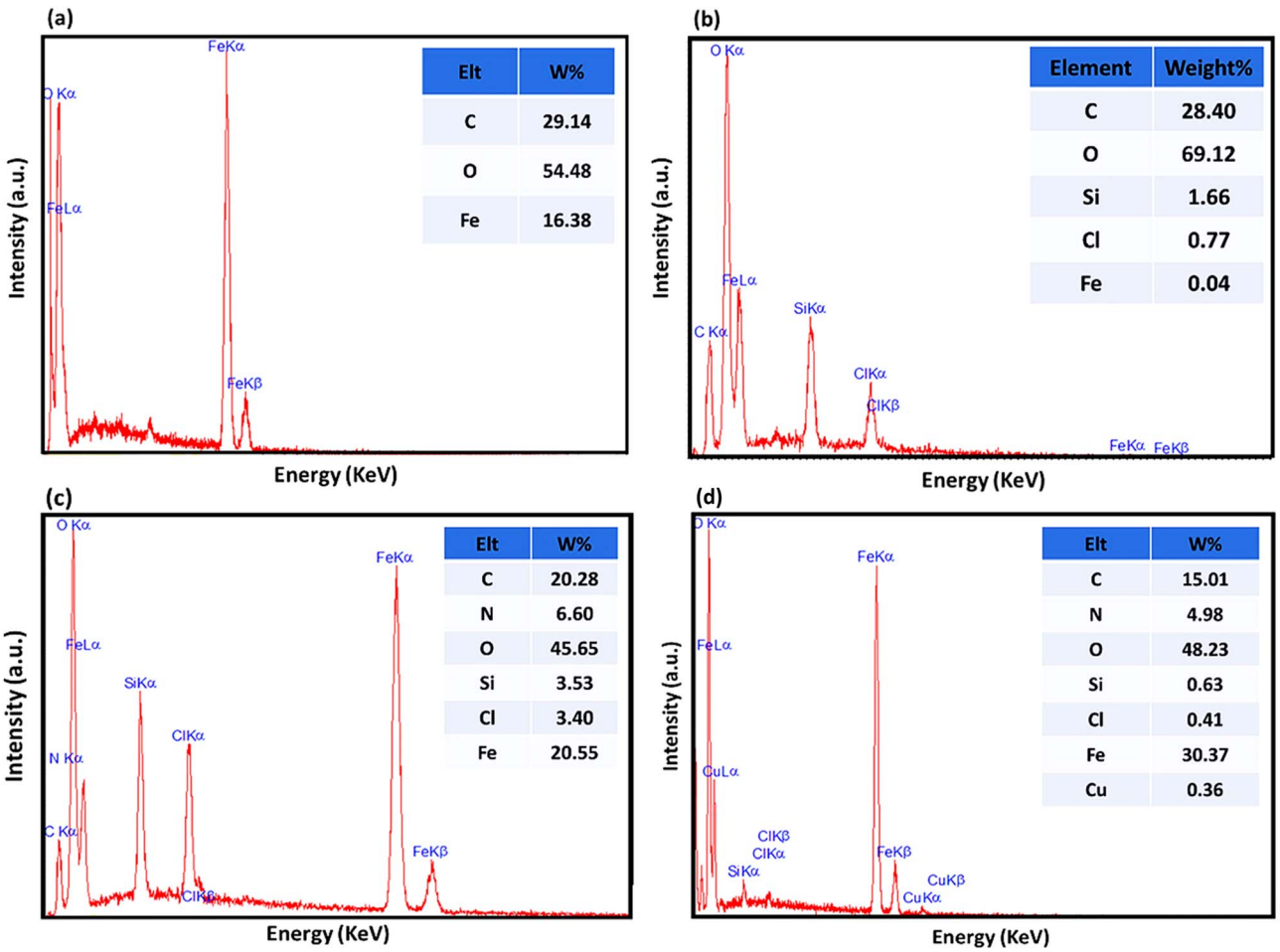

Fig. 2 Results of the energy dispersive X-ray (EDX) analysis of Fe_3O_4@AG (a), Fe_3O_4@AG@CPTMS (b), Fe_3O_4@AG/AP (c), and Fe_3O_4@AG/AP-Cu(I) (d) nanocomposites.

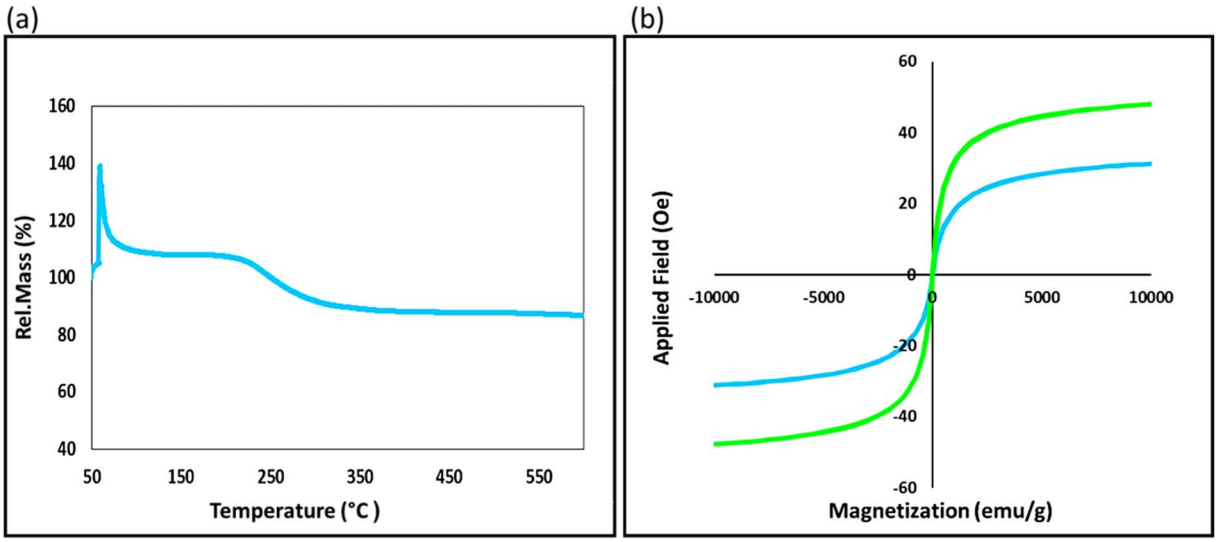

Fig. 3 The TGA of the Fe_3O_4@AG/AP-Cu(I) nanocomposite (a), and the M–H curves of the Fe_3O_4@AG (green curve) and Fe_3O_4@AG/AP-Cu(I) nanocomposites (blue curve) at room temperature (b).

Furthermore, the presence of the natural AG polymer in the catalyst's structure, which possesses an abundance of hydrophilic groups (–OH and –COOH), results in exceptional performance in water as a green solvent. This aspect aligns with the principles of green chemistry and highlights the potential of this innovative catalyst in promoting environmentally conscious practices. The general method of the designed nanocatalyst synthesis is as follows. First, the Fe_3O_4@AG nanopowder was prepared *via* a mixture of the iron(II) and iron(III) chloride solution and AG solution under basic conditions. In this phase, the Fe_3O_4 MNPs are immobilized within the polymer matrix *via* electrostatic interactions between the carboxylic group of AG and the surface hydroxyl group of Fe_3O_4, thereby ensuring optimal stability and functionality. In the second stage, the Fe_3O_4@AG powder was dissolved in dry toluene, and CPTMS was added to it. Then, the solution mixture was refluxed for 24 h. In the third step, the Fe_3O_4@AG@CPTMS solution was dispersed by sonication. CPTMS was employed to attach AP onto the Fe_3O_4@AG composite surface. This procedure was achieved by forming a covalent bond between the hydroxyl groups present on the composite surface and the Si atoms of the CPTMS structure. Next, AP and trimethylamine were added to Fe_3O_4@AG@CPTMS solution in ethanol and refluxed under an N_2 atmosphere. To facilitate the placement of Cu ions, trimethylamine and AP were utilized to activate the amino group within the AP structure and serve as an anchor. In the final step, the fabricated Fe_3O_4@AG/AP magnetic

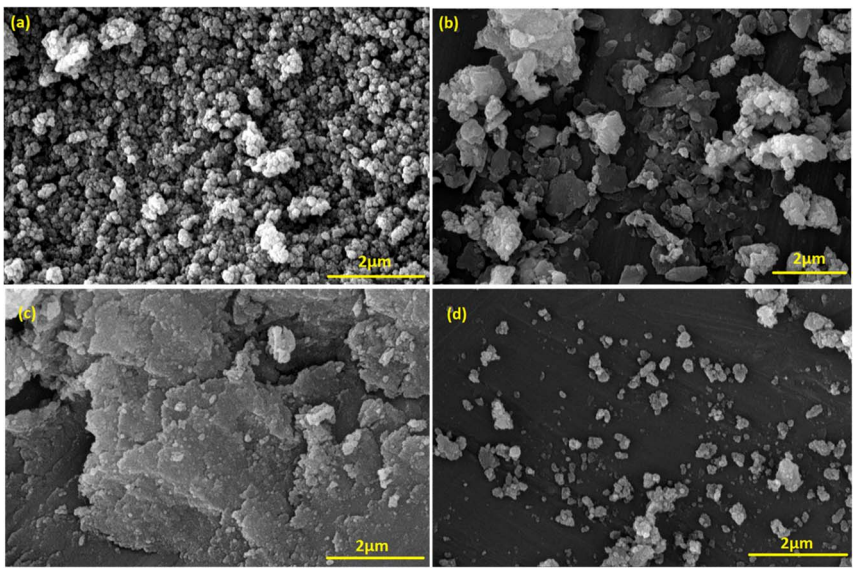

Fig. 4 FESEM images of Fe_3O_4@AG (a), Fe_3O_4@AG@CPTMS (b), Fe_3O_4@AG/AP (c), and Fe_3O_4@AG/AP-Cu(I) (d) nanocomposites.

Table 1 The reaction condition optimization of [1,2,3]-triazole compound synthesis in the presence of the Fe_3O_4@AG/AP-Cu(I) nanocatalyst

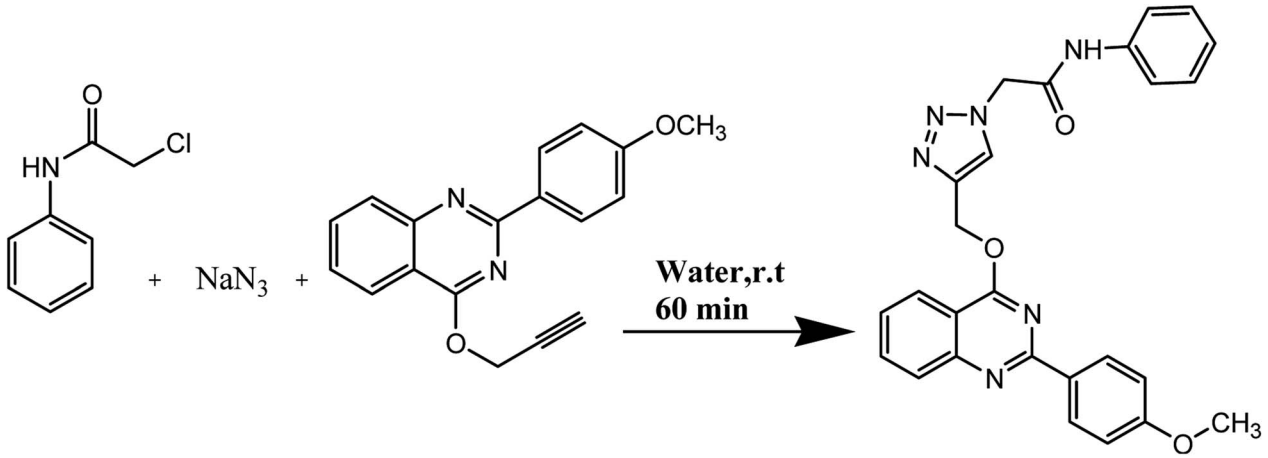

Entry	Catalyst (mg)	Solvent	Temperature (°C)	Time (min)	Yield (%)
1	—	H_2O	r.t.	35	—
2	10	H_2O	r.t.	35	70
3	10	EtOH	r.t.	35	47
4	10	H_2O/EtOH (1 : 1)	r.t.	35	60
5	10	Toluene	r.t.	35	20
6	10	$CHCl_3$	r.t.	35	27
7	10	H_2O : EtOH (1 : 2)	r.t.	35	50
8	10	PEG-400	r.t.	35	Trace
9	10	Isopropanol	r.t.	35	33
10	10	1,4-Dioxane	r.t.	35	15
11	10	CH_3CN(CAN)	r.t.	35	43
12	10	ACN/H_2O	r.t.	35	37
13	20	H_2O	r.t.	35	77
14	30	H_2O	r.t.	35	80
15	40	H_2O	r.t.	35	83
16	50	H_2O	r.t.	35	86
17	70	H_2O	r.t.	35	86
18	50	H_2O	r.t.	45	90
19	50	H_2O	r.t.	60	95
20	50	H_2O	r.t.	75	95
21	50	H_2O	r.t.	90	95
22	50	H_2O	r.t.	120	95
23	50	H_2O	50	60	97
24	50	H_2O	75	60	99
25	50	H_2O	90	60	99
26	50	H_2O	100	60	99

nanocomposite was reacted with CuCl and Cu(I) placed on the AP *via* coordination interaction with N-donor ligands. The preparation process of the Fe_3O_4@AG/AP-Cu(I) magnetic nanocomposite is displayed in Scheme 1. Eventually, the final product was characterized by FTIR, XRD, TGA, EDX, VSM, and FESEM analyses.

3.2. Characterization of the Fe_3O_4@AG/AP-Cu(I) magnetic nanocomposite

3.2.1. FTIR analysis. To characterize the basic functional groups in the structure of Fe_3O_4@AG/AP-Cu(I) magnetic nanocomposite, Fourier-transform infrared (FTIR) spectra of the AG (spectrum I), Fe_3O_4@AG nanopowder (spectrum II), the Fe_3O_4@AG@CPTMS magnetic nanocomposite (spectrum III), the Fe_3O_4@AG/AP magnetic nanocomposite (spectrum IV), and the Fe_3O_4@AG/AP-Cu(I) magnetic nanocomposite (spectrum V) are displayed in Fig. 1a. In spectrum I, the absorbance peaks at around 3422 and 2939 cm^{-1} are related to the stretching vibration of O–H and C–H (hybridization sp^3) bonds. Two strong peaks at 1603 and 1424 cm^{-1} confirm the presence of the COO^- group.[25,100] In spectrum II, the absorbance peak at around 558 cm^{-1} confirms the presence of Fe_3O_4 MNPs in the Fe_3O_4@AG magnetic nanocomposite. In spectrum III, the existent peaks at 1116, 1043, and 2933 cm^{-1} are ascribed to the Si–O and C–H stretching bonds in the CPTMS structure.[101] In

Table 2 Synthesis of [1,2,3]-triazole derivatives in the presence of the Fe_3O_4@AG/AP-Cu(I) nanocomposite

Entry	Alkyne	Sodium azide	2-Chloro-*N*-phenyl-acetamide derivatives	Product	Yield (%)	Number of compounds
1	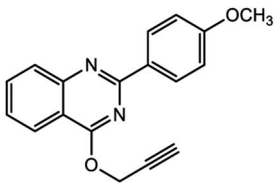	NaN_3	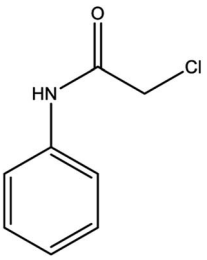	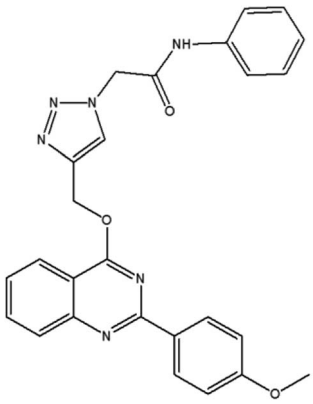	95	**2a**
2	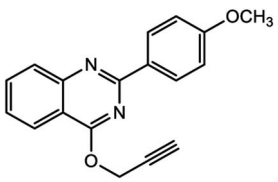	NaN_3	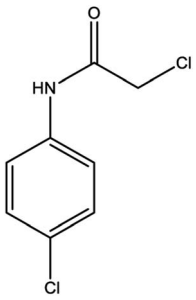	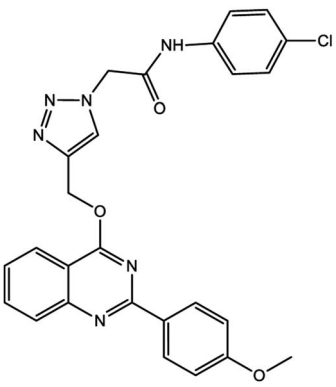	97	**2b**
3	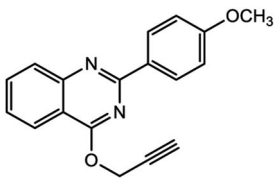	NaN_3	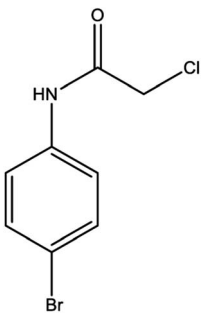	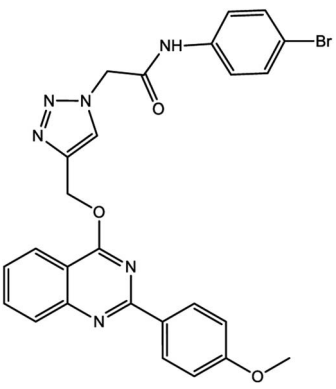	96	**2c**
4	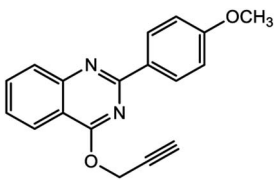	NaN_3	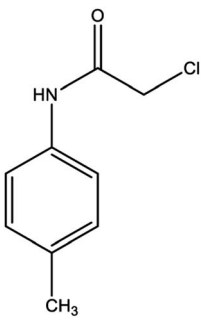	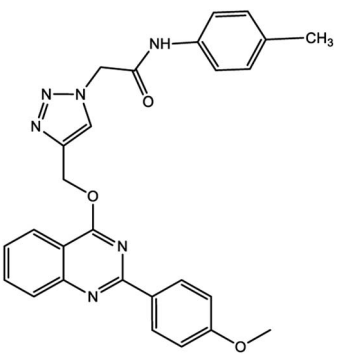	90	**2d**

Table 2 (*Contd.*)

Entry	Alkyne	Sodium azide	2-Chloro-*N*-phenyl-acetamide derivatives	Product	Yield (%)	Number of compounds
5	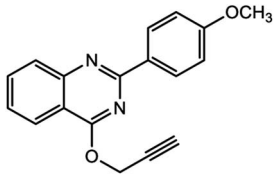	NaN_3	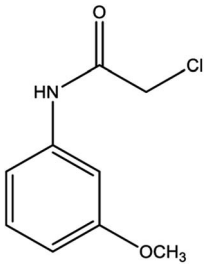	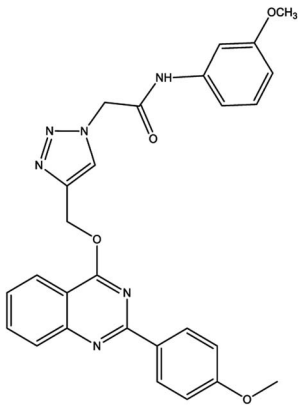	96	**2e**
6	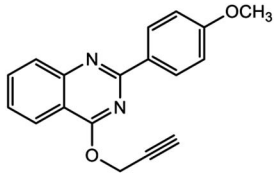	NaN_3	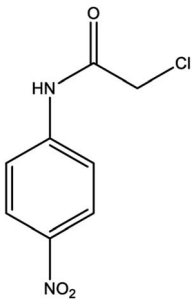	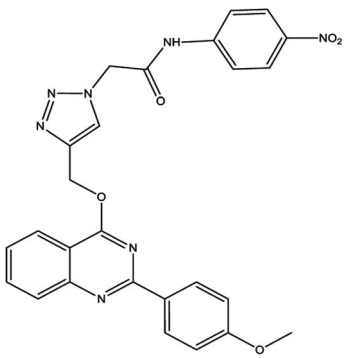	97	**2f**
7	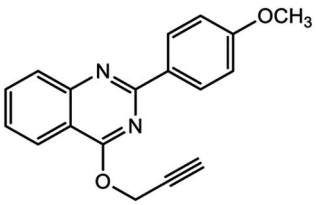	NaN_3	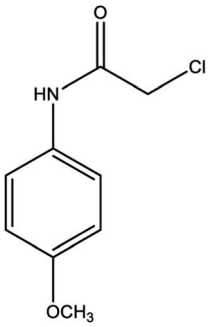	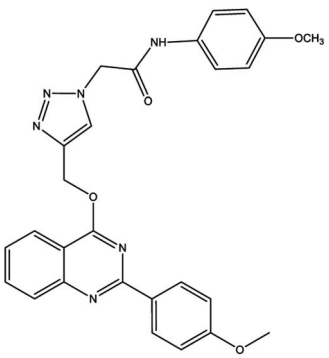	97	**2g**

spectrum IV, the characterized absorption peaks occurring at 1690–1560 cm^{-1} and 1405 cm^{-1} are attributed to the bending vibration of the N–H bond, and stretching vibration of C=N, and C–N bonds of AP in the structure of the Fe_3O_4@AG/AP magnetic nanocomposite.[102–104] In addition, the stretching vibrations of Cu–O bonds in the structure of the Fe_3O_4@AG/AP-Cu(I) nanocomposite appear at ~635 cm^{-1}, which overlapped with the peak related to the stretching vibrations of Fe–O bonds.[14]

3.2.2. XRD analysis. The XRD patterns of the Fe_3O_4@AG (I), Fe_3O_4@AG@CPTMS (II), Fe_3O_4@AG/AP (III), and Fe_3O_4@AG/AP-Cu(I) (IV) nanocomposites are illustrated in Fig. 1b. All diffraction patterns have a fine match with the reference pattern of the Fe_3O_4 MNPs. It confirms that they have been well distributed onto the AG textures. These peaks appear at 2θ = 30.22°, 35.55°, 43.28°, 53.56°, 57.19°, and 62.81° that are related to the (220), (311), (400), (422), (511), and (400) Miller indices, respectively, with 00-19-0629 JCPDS card number.[105] In the diffraction pattern attributed to the Fe_3O_4@AG/AP-Cu(I) (IV) nanocomposite, three essential peaks at 2θ = 43.28°, 50.18°, and 74.68° with (111), (200), and (220) Miller indices confirmed the presence of Cu NPs in the final product (JCPDS card no. 00-004-0836).[106]

3.2.3. EDX analysis. Energy-dispersive X-ray (EDX) analysis was also performed to characterize the prepared compositions' constituent elements, as shown in Fig. 2. Based on Fig. 2a,

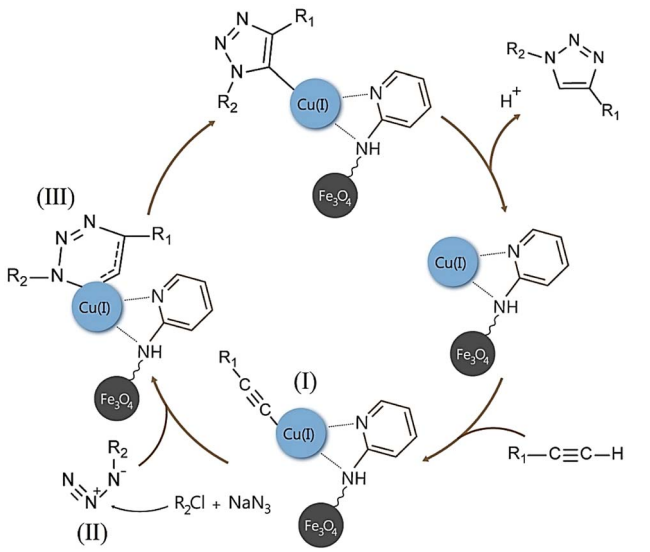

Scheme 2 The synthesis reaction mechanism of triazole derivatives in the presence of the Fe_3O_4@AG/AP-Cu(I) nanocomposite.

oxygen, carbon, and iron peaks confirm the presence of AG as a natural polymer and Fe_3O_4 MNPs in the structure of Fe_3O_4@AG nanocomposite. In Fig. 2b, the assigned Si and Cl peaks can be related to the presence of the CPTMS structure and its successful connection to the Fe_3O_4@AG nanocomposite. In Fig. 2c, the presence of N, C, and O peaks in the spectrum is attributed to the AG and AP structures. In addition, the other peaks, such as those of Fe, Si, and Cl, are related to Fe_3O_4 and CPTMS in the Fe_3O_4@AG/AP nanocomposite structure. The EDX spectrum of the final product shows the poor peaks of Cu that confirm the interaction between N atoms in the AP and Cu NPs and the formation of the Fe_3O_4@AG/AP-Cu(I) nanocomposite (Fig. 2d).

3.2.4. TGA analysis. The thermogravimetric analysis (TGA) was performed in a thermal range of 50–600 °C to evaluate the thermal stability of the prepared Fe_3O_4@AG/AP-Cu(I) nanocomposite (Fig. 3a). As can be seen, initially, a weight increase occurs with the increase in temperature up to about 60 °C, which can occur due to the device's buoyancy effect.[107] As the temperature increases, a 13.0% weight decrease occurs at 214–388 °C, which can be attributed to the decomposition of organic compounds such as the polysaccharide backbone and AP structure.[108] Accordingly, the prepared catalyst will not be destroyed under the experimental conditions because the reaction temperature was about 100 °C.

3.2.5. VSM analysis. Vibrating-sample magnetometry (VSM) was used to evaluate the magnetic properties of the obtained products, as illustrated in Fig. 3b. As can be seen, a comparison has been made between Fe_3O_4@AG and Fe_3O_4@AG/AP-Cu(I) nanocomposites. Both samples rendered a superparamagnetic behavior. Initially, the saturation magnetization value of NPs coated with natural polymer was recorded as 48.06 emu g^{-1} (green curve). Subsequently, the magnetic characteristics of Fe_3O_4@AG were analyzed after the attachment of CPTMS, AP, and Cu ions onto its surface, resulting in a decrease of *ca.* 17 emu g^{-1}, ultimately reaching a value of 31.21 emu g^{-1} for the Fe_3O_4@AG/AP-Cu(I) nanocomposite (blue curve). This significant reduction corroborates the effective functionalization of the AG surface with copper ions. The saturation magnetization value of the final nanocomposite is sufficient for performing a magnetically suitable separation process.

3.2.6. FESEM analysis. The FESEM analysis was performed to identify the morphology of the products step by step and is illustrated in Fig. 4. In Fig. 4a, the spherical morphology of Fe_3O_4 MNPs can be seen. The image reveals a homogeneous distribution of NPs within the polymer matrix, exhibiting a consistent morphology and dimensions. The mean particle diameter was determined to be 65.87 nm. Fig. 4b shows particle agglomeration that occurs after adding CPTMS. This can be attributed to the adhesive nature of the silicate compounds.[15] The spherical morphology is completely lost after adding AP as anchor molecules, and a sheet structure appears (Fig. 4c). In the final step, the Cu ions were placed on the surface of the Fe_3O_4@AG/AP nanocomposite (Fig. 4d).

3.3. Application of the Fe_3O_4@AG/AP-Cu(I) nanocomposite

3.3.1. Optimization of essential parameters in a catalyzed click reaction with the Fe_3O_4@AG/AP-Cu(I) nanocomposite. The effective and essential parameters such as solvent, reaction time, temperature, and product efficiency were evaluated for promoting catalyzed [1,2,3]-triazole compound preparation reactions. In this regard, 1.0 mmol of alkyne, 1.1 mmol of sodium azide, and 1.0 mmol of 2-chloro-*N*-phenyl-acetamide derivatives were applied under different conditions, and experiments were performed in the presence and absence of several amounts of the Fe_3O_4@AG/AP-Cu(I) nanocatalyst. The reaction was investigated in water, ethanol, toluene, acetonitrile, chloroform, isopropanol, and 1,4-dioxane solvents. The results showed that the highest efficiency of 95.0% was obtained in water solvent and at room temperature (Table 1). Increasing the catalyst dosage to 50.0 mg was very effective in enhancing reaction efficiency and had a direct relationship. The evaluation of the laboratory results showed that the designed nanocatalyst having AG chains as a natural hydrophilic polymer in its structure was dispersed well in a water solvent. Therefore, Fe_3O_4@AG/AP-Cu(I) particles can interact significantly with available reactants in water solvents and increase the reaction efficiency.[17] The catalytic process is heavily influenced by the solvent's characteristics, particularly its dipolarity or polarity, as well as its proticity and basicity, which determine its ability to donate and accept hydrogen bonds. In the prepared nanocatalyst structure, the AG natural polymer is endowed with numerous hydrophilic groups, such as –OH and –COOH, which enable it to achieve a superior dispersion in the solvent by forming hydrogen bond networks with water molecules.[109,110] These interactions enhance reaction efficiency, surpassing that of other solvents like toluene, acetonitrile, and chloroform, which were subjected to comparative testing. Furthermore, the superior catalytic performance observed in aqueous solvents, as

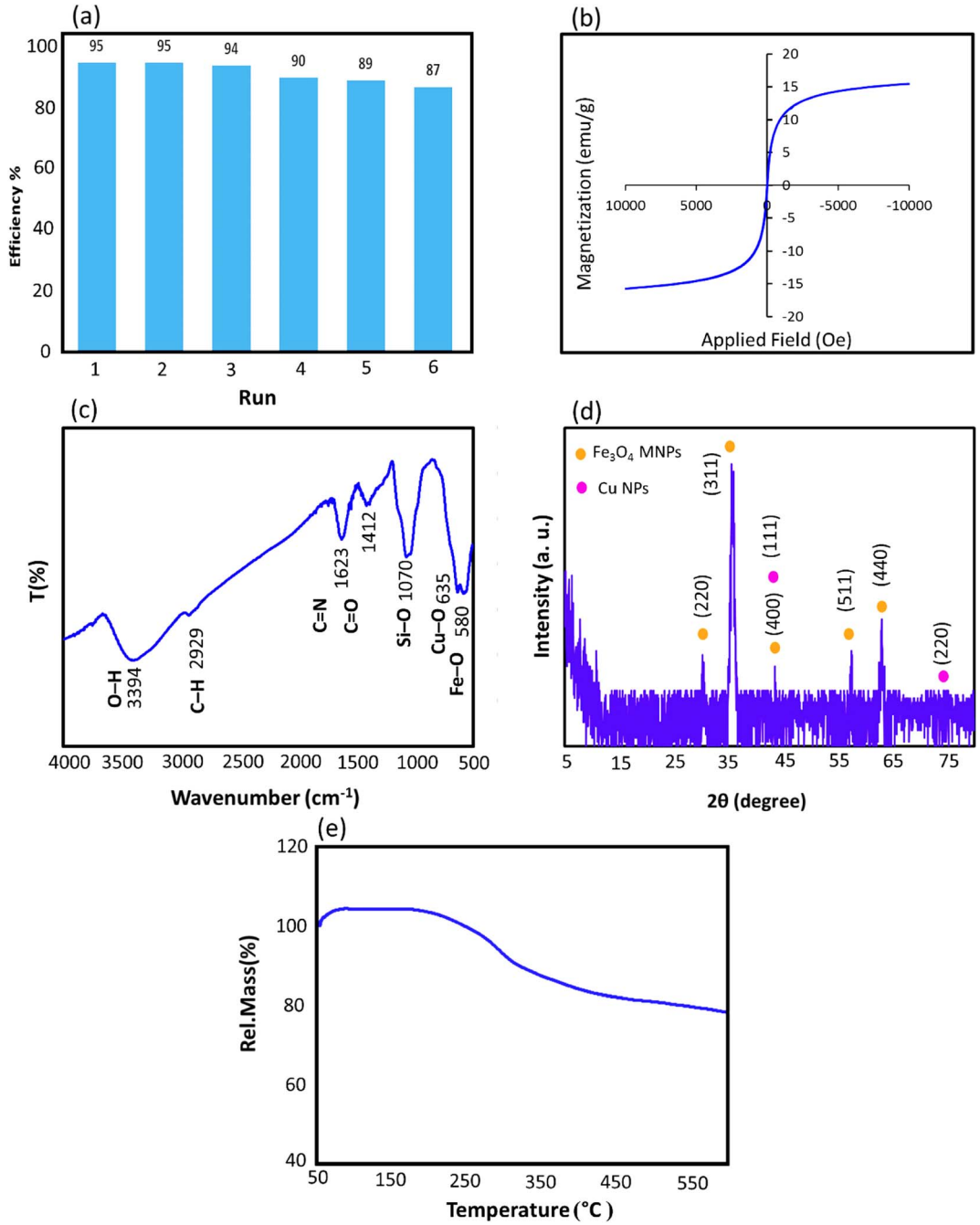

Fig. 5 Catalyst recycling results after six consecutive cycles of [1,2,3]-triazole compound synthesis (a), VSM (b), FTIR (c), XRD (d), and TGA (e) analyses of the nanocatalyst after six sequential recycling cycles.

opposed to other protic solvents like ethanol and isopropanol, can be attributed to the elevated dipolarity of water, which is because two hydrogen atoms are covalently bonded to a single oxygen atom in the water molecular structure. In contrast, each alcohol molecule only has one hydrogen atom attached to an oxygen atom, with the remaining portion being an alkyl group.[111]

3.3.2. Evaluation of the catalytic efficiency of the Fe_3O_4@AG/AP-Cu(I) nanocomposite in the [1,2,3]-triazole click reaction. To investigate the performance of the prepared catalyst in the click reaction, a wide range of 2-chloro-*N*-phenylacetamide derivatives with alkyne and sodium azide were used to synthesize [1,2,3]-triazole derivatives. All reactions were performed under optimal conditions, and the results showed high yields at 60 min, 50.0 mg catalyst dosage, and room temperature (Table 2). The ^{1}H-NMR and ^{13}C-NMR spectra of these compounds are shown in the ESI File (2a–2e).†

3.3.3. Suggested mechanism. As exhibited in Scheme 2, the proposed mechanism of this reaction is a cyclic and multi-stage reaction in which copper stabilized in an AG polysaccharide

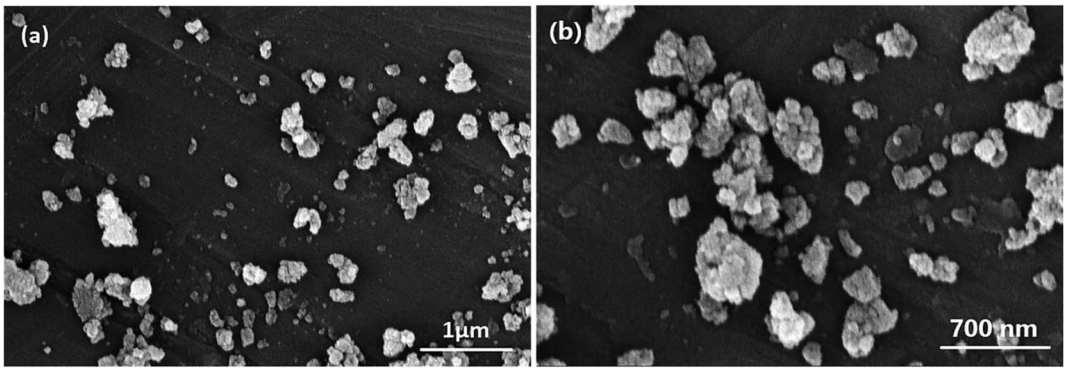

Fig. 6 FESEM images of the nanocatalyst after six sequential recycling cycles on two scales, 1.0 μm (a) and 700.0 nm (b).

substrate plays a fundamental role in forming carbon–nitrogen bonds. At the beginning of the catalytic cycle, the alkyne in the presence of copper stabilized in the natural polymer substrate is converted into copper acetylide (**1**), an active compound, during a rapid reaction. Also, sodium azide binds to 2-chloro-*N*-phenylacetamide through formation of a carbon–nitrogen bond and leaving a chlorine atom, constituting an alkyl azide compound (**2**). Then, the copper(I) acetylide structure reacts with the formed alkyl azide, and 1, 3-dipolar cyclization is performed. This process leads to the formation of the final product (**3**).

3.3.4. Catalyst recycling. Catalyst recyclability was evaluated to investigate economic and environmental aspects. For this purpose, the prepared nanocatalyst was separated with an external magnet after multicomponent synthesis and washed several times with distilled water and ethanol. Then, it was reused. The results showed that this nanocatalyst acted with high efficiency after even six runs of recycling, and a trivial reduction in the yield was observed. Therefore, it can be concluded that the prepared nanocatalyst can be introduced as a suitable candidate for increasing efficiency and reducing the desired reaction time (Fig. 5a). In order to assess the integrity of the catalyst that was prepared, a series of advanced analytical techniques were employed after six runs of successive recycling. The VSM, FTIR, XRD, TGA, and FESEM analyses were conducted to determine the structural properties of the catalyst. The VSM analysis results indicated that the catalyst's saturation magnetism following six runs was 15.46 emu g^{-1}, a satisfactory value for effectively isolating the catalyst from the reaction solution (Fig. 5b). The FTIR analysis revealed that all the functional groups associated with the synthesized catalyst's structure were well-preserved, indicating that the structure has remained intact even after repeated washing and six reaction cycles. Hence, the structure has not collapsed (Fig. 5c). The XRD pattern shows the presence of Fe_3O_4 MNPs and Cu NPs in the catalyst structure (Fig. 5d). Furthermore, the TGA analysis demonstrates that the prepared nanocomposite exhibits exceptional thermal stability up to 240 °C, comparable to that of the original sample before recycling (Fig. 5e). In addition, the FESEM images obtained from the sample after undergoing six reaction cycles exhibit preserved catalyst integrity indistinguishable from that in the FESEM images obtained before multiple runs (Fig. 6a and b).

For the hot test filtration execution, the desired solvent (distilled water) was warmed to reach its boiling point (100 °C). Afterward, the boiled solvent (10.0 mL) was poured on the Fe_3O_s@AG/AP-Cu(I) nanocatalyst, and after cooling down the reaction temperature to 25 °C, it was filtered by using filter paper. In this regard, the filtration paper was rinsed with boiling water, the reaction mixture was filtered, and the ICP test of the supernatant was carried out. The ICP-OES test was performed to specify the Fe^{3+} and Cu^{+} ion amounts released into the supernatant solution under optimized reaction conditions. According to the ICP test results, the released Fe^{3+} and Cu^{+} ion concentration in the supernatant solution was measured to be 0.21 ppm and 95.22 ppm, respectively, which can be ascribed to the insufficient magnetic isolation of the magnetic nanocatalyst from the reaction mixture after the accomplishment of the catalytic reaction. Therefore, the meager leaching percentage of the Fe_3O_4@AG/AP-Cu(I) nanocatalyst or Fe^{3+} and Cu^{+} ions into the reaction solution can be neglected; hence, the magnetic nanocatalyst can be employed many times without a decline in the catalytic performance, as authenticated by recyclability tests.

3.3.5. Comparisons of the fabricated Fe_3O_4@AG/AP-Cu(I) nanocomposite with other catalytic systems. Here, a general comparison has been made between the designed nanocatalyst and other previously prepared systems that can accelerate the synthesis of triazole derivatives with acceptable yields. As shown in Table 3, the prepared catalyst has significant advantages compared to other catalysts described in the following description. High efficiency (95.0%) has occurred in an appropriate period of 60 min, which was a better performance than that of other catalyst systems (entries 1, 2, and 5). In addition, due to the importance of green chemistry, it is very important to design catalytic systems based on natural and low-toxic materials. In this work, the prepared nanocatalyst is based on AG as a natural hydrophilic polymer, which can cover this issue well compared to other designed catalysts (entries 2, 4, and 5). In addition, this nanocatalyst has the highest efficiency in water as a green solvent compared with the others (entry 1). One of the notable advantages of the designed nanocatalyst is its high performance at ambient temperature, which makes it highly

Table 3 The comparison of the prepared Fe_3O_4@AG/AP-Cu(I) nanocatalyst and previously reported nanocatalytic systems for click chemistry azide-alkyne cycloaddition

Entry	Catalyst	Condition	Cat.[a] (mg)	Time(min)	Yield (%)	Ref.
1	Cellulose–copper(II) oxide	r.t./EtOH	30	10	92	112
2	Au–Cu core–shell nanocubes	50 °C/H_2O	3	180	91	113
3	FBPs-CuBr[b]	80 °C/H_2O/under MW	5.50	30	96	114
4	CuO–HMSS[c]	80 °C/H_2O	40	8	96	115
5	Fe_3O_4@TiO_2/Cu_2O	Reflux/H_2O	20	15	93	116
6	Fe_3O_4@AG/AP-Cu(I)	r.t./H_2O	50	60	95	This work

[a] Catalyst amount. [b] Waste fishbone powder supported CuBr. [c] CuO included hollow mesoporous silica spheres.

different from many previously designed catalysts and aimed at preventing energy loss (entries 2, 3, 4, and 5).

4. Conclusion

The click reaction has emerged as a crucial one-pot method for synthesizing triazole heterocyclic compounds, which are highly significant in pharmaceuticals. We have developed a heterogeneous and hydrophilic nanocatalyst to synthesize [1,2,3]-triazole derivatives. The nanocatalyst is based on an AG natural polymer, which enhances its biocompatibility and reduces its toxicity, thereby conforming to the principles of green chemistry. In addition, the nanocatalyst exhibits magnetic properties, which enable it to be easily separated from the reaction flask and reused after washing. The reaction was carried out in water as a green solvent at ambient temperature, and the efficiency of the nanocatalyst was found to be high. Various structural analyses (FTIR, EDX, XRD, TGA, VSM, and FESEM) were conducted to confirm the characteristics of the designed nanocatalyst, and VSM analysis determined the saturation magnetization value to be 31.21 emu g^{-1}. The reaction conditions were optimized, and a reaction yield of 95.0% was achieved for 50.0 mg of catalyst at 60 min. The performance of the nanocatalyst was investigated for [1,2,3]-triazole derivative synthesis, and the results demonstrated its excellent catalytic performance (Table 2). Finally, the recyclability of the nanocatalyst was examined after six successive runs, and all results confirmed the structural stability.

Author contributions

N. Khaleghi: conceptualization and bench work (all synthesis steps), A. Mohammadi: writing the manuscript and preparation of supplementary files,† M. Forouzandeh-Malati: bench work (all synthesis steps), planning to carry out synthesis steps and analyses, Z. Sadat Mojtabapour: bench work (2.2, 2.3, 2.4, and 2.5 Sections of nanocatalyst preparation), analyses and supplying the required materials, F. Ganjali: bench work (all synthesis steps), analysis, and writing the Materials and equipment section, S. Z. Rashvandi: graphics, Simindokht Zarei-Shokat: bench work (2.2, 2.3, 2.4, and 2.5 Sections of nanocatalyst preparation) and follow up to prepare materials, A. Kashtiaray: revision, R. Taheri-Ledari: supervision, project administration, reviewing, editing, and revision, and A. Maleki: supervision, and financial support.

Conflicts of interest

The authors have no conflict of interest.

Acknowledgements

The authors gratefully acknowledge the partial support from the Iran University of Science and Technology (IUST).

References

1 P. Shiri and J. Aboonajmi, *Beilstein J. Org. Chem.*, 2020, **16**, 551–586.
2 F. Laffafchi, M. Tajbakhsh, Y. Sarrafi, B. Maleki and M. Ghani, *Polycyclic Aromat. Compd.*, 2022, **43**, 1–17.
3 E. Arefi, A. Khojastehnezhad and A. Shiri, *Sci. Rep.*, 2021, **11**, 20514.
4 C. Zhou, Y. Wang, E. Wong, E. Fonkem, T. Hsieh, J. Wu and E. Wu, *Curr. Med. Chem.*, 2012, **19**, 239–280.
5 V. I. Böhmer, W. Szymanski, K. O. van den Berg, C. Mulder, P. Kobauri, H. Helbert and P. H. Elsinga, *Eur. J. Chem.*, 2020, **26**, 10871–10881.
6 A. Dondoni, *Chem.–Asian J.*, 2007, **2**, 700–708.
7 K. Kowalski, *Coord. Chem. Rev.*, 2023, **479**, 214996.
8 V. D. Bock, H. Hiemstra and J. H. Van Maarseveen, *Eur. J. Org. Chem.*, 2006, **2006**, 51–68.
9 V. K. Tiwari, B. B. Mishra, K. B. Mishra, N. Mishra, A. S. Singh and X. Chen, *Chem. Rev.*, 2016, **116**, 3086–3240.
10 R. U. Islam, A. Taher, M. Choudhary, M. J. Witcomb and K. Mallick, *Dalton Trans.*, 2015, **44**, 1341–1349.
11 T. Kitanosono, K. Masuda, P. Xu and S. Kobayashi, *Chem. Rev.*, 2018, **118**, 679–746.
12 C. W. Tornøe, C. Christensen and M. Meldal, *J. Org. Chem.*, 2002, **67**, 3057–3064.
13 G. Molteni, C. L. Bianchi, G. Marinoni, N. Santo and A. Ponti, *New J. Chem.*, 2006, **30**, 1137–1139.
14 L. Jiang, Z. Wang, S.-Q. Bai and T. A. Hor, *Dalton Trans.*, 2013, **42**, 9437–9443.
15 V. O. Rodionov, S. I. Presolski, S. Gardinier, Y.-H. Lim and M. Finn, *J. Am. Chem. Soc.*, 2007, **129**, 12696–12704.
16 J. Y. Kim, J. C. Park, H. Kang, H. Song and K. H. Park, *ChemComm*, 2010, **46**, 439–441.
17 R. ta-Ledari, M. Saeidirad, F. S. Qazi, A. Fazeli, A. Maleki and A. E. Shalan, *RSC Adv.*, 2021, **11**, 25284–25295.

18 N. Kerru, S. V. Bhaskaruni, L. Gummidi, S. N. Maddila and S. B. Jonnalagadda, *Synth. Commun.*, 2019, **49**, 2437–2459.
19 A. Maleki, R. Taheri-Ledari, R. Ghalavand and R. Firouzi-Haji, *J. Phys. Chem. Solids*, 2020, **136**, 109200.
20 A. Maleki, R. Taheri-Ledari and M. Soroushnejad, *ChemistrySelect*, 2018, **3**, 13057–13062.
21 A. Poursattar Marjani, F. Asadzadeh and A. Danandeh Asl, *Sci. Rep.*, 2022, **12**, 22173.
22 A. Ghorbani-Choghamarani, H. Aghavandi and S. M. Talebi, *Sci. Rep.*, 2022, **12**, 20775.
23 S. Mirani Nezhad, E. Nazarzadeh Zare, A. Davarpanah, S. A. Pourmousavi Seied Ali Pourmousavi, M. Ashrafizadeh Milad Ashrafizadeh and A. P. Kumar, *Molecules*, 2022, **27**, 1748.
24 Z. Hajizadeh, K. Valadi, R. Taheri-Ledari and A. Maleki, *ChemistrySelect*, 2020, **5**, 2441–2448.
25 R. Taheri-Ledari, S. M. Hashemi and A. Maleki, *RSC Adv.*, 2019, **9**, 40348–40356.
26 R. Taheri-Ledari, A. Maleki, E. Zolfaghari, M. Radmanesh, H. Rabbani, A. Salimi and R. Fazel, *Ultrason. Sonochem.*, 2020, **61**, 104824.
27 R. Taheri-Ledari, K. Valadi, S. Gharibi and A. Maleki, *Mater. Res. Bull.*, 2020, **130**, 110946.
28 R. Taheri-Ledari and A. Maleki, *New J. Chem.*, 2021, **45**, 4135–4146.
29 V. Adimule, B. C. Yallur, M. M. Pai, S. R. Batakurki and S. S. Nandi, *Top. Catal.*, 2022, DOI: **10.1007/s11244-022-01672-9**.
30 V. Soltaninejad, M. R. Ahghari, R. Taheri-Ledari and A. Maleki, *Langmuir*, 2021, **37**, 4700–4713.
31 S. Naghash-Hamed, N. Arsalani and S. B. Mousavi, *Sci. Rep.*, 2023, **13**, 3329.
32 R. Taheri-Ledari, S. S. Mirmohammadi, K. Valadi, A. Maleki and A. E. Shalan, *RSC Adv.*, 2020, **10**, 43670–43681.
33 F. FarhKhanmohammadi-Sarabi, A. Ghorbani-Choghamarani, H. Aghavandi and M. A. Zolfigol, *New J. Chem.*, 2023, **47**, 4252–4266.
34 A. Bahadoran, S. Ramakrishna, B. Oryani, L. Ahmed Al-Keridis, H. Rashidi Nodeh and S. Rezania, *Fuel*, 2022, **319**, 123858.
35 R. Taheri-Ledari and A. Maleki, in *Magnetic Nanoparticle-Based Hybrid Materials*, Elsevier, 2021, pp. 619–636.
36 R. Taheri-Ledari, F. R. Asl, M. Saeidirad, A. Kashtiaray and A. Maleki, *Sci. Rep.*, 2022, **12**, 4719.
37 P. Guardia, A. Labarta and X. Batlle, *J. Phys. Chem. C*, 2011, **115**, 390–396.
38 M. Zhu and G. Diao, *Nanoscale*, 2011, **3**, 2748–2767.
39 Q. Li, H. Li, V. G. Pol, I. Bruckental, Y. Koltypin, J. Calderon-Moreno and A. Gedanken, *New J. Chem.*, 2003, **27**, 1194–1199.
40 X. Chen, K. M. Unruh, C. Ni, B. Ali, Z. Sun, Q. Lu and J. Q. Xiao, *J. Phys. Chem. C*, 2011, **115**, 373–378.
41 T. Hyeon, *Commun. Chem.*, 2003, **8**, 927–934.
42 M. D. Nguyen, H. V. Tran, S. Xu and T. R. Lee, *Appl. Sci.*, 2021, **11**, 11301.
43 Y. C. Li, Y. S. Lin, P. J. Tsai, C. T. Chen, W. Y. Chen and Y. C. Chen, *Anal. Chem.*, 2007, **79**, 7519–7525.
44 J. Chen, L. Xu, W. Li and X. Gou, *Adv. Mater.*, 2005, **17**, 582–586.
45 N. A. Frey, S. Peng, K. Cheng and S. Sun, *Chem. Soc. Rev.*, 2009, **38**, 2532–2542.
46 S. Bikas, A. Poursattar Marjani, S. Bibak and H. Sarreshtehdar Aslaheh, *Sci. Rep.*, 2023, **13**, 2564.
47 H. Boroumand, H. Alinezhad, B. Maleki and S. Peiman, *Polycyclic Aromat. Compd.*, 2022, 1–17.
48 M. Jarrahi, B. Maleki and R. Tayebee, *RSC Adv.*, 2022, **12**, 28886–28901.
49 M. Tarahomi, H. Alinezhad and B. Maleki, *Appl. Organomet. Chem.*, 2019, **33**, e5203.
50 R. Taheri-Ledari, F. S. Qazi, M. Saeidirad and A. Maleki, *Sci. Rep.*, 2022, **12**, 14865.
51 N. Khaleghi, M. Forouzandeh-Malati, F. Ganjali, Z. Rashvandi, S. Zarei-Shokat, R. Taheri-Ledari and A. Maleki, *Sci. Rep.*, 2023, **13**, 5225.
52 F. Ganjali, A. Kashtiaray, S. Zarei-Shokat, R. Taheri-Ledari and A. Maleki, Functionalized hybrid magnetic catalytic systems on micro-and nanoscale utilized in organic synthesis and degradation of dyes, *Nanoscale Adv.*, 2022, **4**, 1263–1307.
53 M. Ghani, S. Khodkavandi, Z. Jafari, B. Maleki and H. F. Tabari, *Microchem. J.*, 2023, **187**, 108368.
54 D. Shi, *Adv. Funct. Mater.*, 2009, **19**, 3356–3373.
55 R. Qiao, C. Yang and M. Gao, *J. Mater. Chem.*, 2009, **19**, 6274–6293.
56 R. Taheri-Ledari and A. Maleki, *J. Pept. Sci.*, 2020, **26**, e3277.
57 R. Taheri-Ledari, E. Zolfaghari, S. Zarei-Shokat, A. Kashtiaray and A. Maleki, *Commun. Biol.*, 2022, **5**, 995.
58 M. Peyvandtalab, E. N. Zare, M. Jabbari and G. Heidari, *Eur. Polym. J.*, 2023, **186**, 111862.
59 W. Zhang, R. Taheri-Ledari, Z. Hajizadeh, E. Zolfaghari, M. R. Ahghari, A. Maleki and Y. Tian, *Nanoscale*, 2020, **12**, 3855–3870.
60 R. Taheri-Ledari, J. Rahimi and A. Maleki, *Mater. Res. Express*, 2020, **7**, 015067.
61 R. Taheri-Ledari, W. Zhang, M. Radmanesh, S. S. Mirmohammadi, A. Maleki, N. Cathcart and V. Kitaev, *Small*, 2020, **16**, 2002733.
62 M. Zhu and G. Diao, *J. Phys. Chem. C*, 2011, **115**, 18923–18934.
63 A. H. Lu, E. E. Salabas and F. Schüth, *Angew. Chem., Int. Ed.*, 2007, **46**, 1222–1244.
64 U. Jeong, X. Teng, Y. Wang, H. Yang and Y. Xia, *Adv. Mater.*, 2007, **19**, 33–60.
65 A. S. Teja and P. Y. Koh, *Prog. Cryst. Growth Charact. Mater.*, 2009, **55**, 22–45.
66 A. Maleki, S. Gharibi, K. Valadi and R. Taheri-Ledari, *J. Phys. Chem. Solids*, 2020, **142**, 109443.
67 S. S. Soltani, R. Taheri-Ledari, S. M. F. Farnia, A. Maleki and A. Foroumadi, *RSC Adv.*, 2020, **10**, 23359–23371.
68 A. Maleki, R. Taheri-Ledari and R. Ghalavand, *Comb. Chem. High Throughput Screening*, 2020, **23**, 119–125.
69 J. Rahimi, R. Taheri-Ledari and A. Maleki, *Curr. Org. Synth.*, 2020, **17**, 288–294.

70 V. Soltaninejad, M. R. Ahghari, R. Taheri-Ledari, A. Maleki and A. E. Shalan, *J. Mol. Struct.*, 2022, **1256**, 132456.
71 A. Islam, G. Phillips, A. Sljivo, M. Snowden and P. Williams, *Food Hydrocolloids*, 1997, **11**, 493–505.
72 P. Supriya, B. T. V. Srinivas, K. Chowdeswari, N. V. S. Naidu and B. Sreedhar, *Mater. Chem. Phys.*, 2018, **204**, 27–36.
73 C. M. Niemeyer, *Angew. Chem., Int. Ed.*, 2001, **40**, 4128–4158.
74 E. Katz and I. Willner, *Angew. Chem., Int. Ed.*, 2004, **43**, 6042–6108.
75 R. Bandyopadhyaya, E. Nativ-Roth, O. Regev and R. Yerushalmi-Rozen, *Nano Lett.*, 2002, **2**, 25–28.
76 V. Kattumuri, K. Katti, S. Bhaskaran, E. J. Boote, S. W. Casteel, G. M. Fent, D. J. Robertson, M. Chandrasekhar, R. Kannan and K. V. Katti, *Small*, 2007, **3**, 333–341.
77 K. P. Velikov, G. E. Zegers and A. van Blaaderen, *Langmuir*, 2003, **19**, 1384–1389.
78 D. N. Williams, K. A. Gold, T. R. P. Holoman, S. H. Ehrman and O. C. Wilson, *J. Nanopart. Res.*, 2006, **8**, 749–753.
79 S. Amirnejat, A. Nosrati, S. Javanshir and M. R. Naimi-Jamal, *Int. J. Biol. Macromol.*, 2020, **152**, 834–845.
80 M. Anvari and D. Chung, *Food Hydrocolloids*, 2016, **60**, 516–524.
81 I. V. Machado, J. R. Dos Santos, M. A. Januario and A. G. Corrêa, *Ultrason. Sonochem.*, 2021, **78**, 105704.
82 H. T. Nguyen, V. A. Truong and P. H. Tran, *RSC Adv.*, 2020, **10**, 25358–25363.
83 A. Maleki, Z. Hajizadeh and K. Valadi, *Green Chem. Lett. Rev.*, 2021, **14**, 62–72.
84 G. Bosica and R. Abdilla, *Catalysts*, 2022, **12**, 725.
85 S. Chaturvedi, P. N. Dave and N. K. Shah, *J. Saudi Chem. Soc.*, 2012, **16**, 307–325.
86 J. Cheng, J. Zhou, Z. Wang and M. Zhang, *Catal. Sci. Technol.*, 2020, **10**, 6387–6392.
87 L. Wang, T. Chen, J. Zhang, Y. Jiao, J. Wang, Q. Zhu and X. Li, *Fuel*, 2020, **268**, 117384.
88 M. Filella and J. Buffle, *Colloids Surf., A*, 1993, **73**, 255–273.
89 M. Faraji, Y. Yamini, A. Saleh, M. Rezaee, M. Ghambarian and R. Hassani, *Anal. Chim. Acta*, 2010, **659**, 172–177.
90 M.-N. Chen, L.-P. Mo, Z.-S. Cui and Z.-H. Zhang, *Curr. Opin. Green Sustainable Chem.*, 2019, **15**, 27–37.
91 S. Berensmeier, *Appl. Microbiol. Biotechnol.*, 2006, **73**, 495–504.
92 A. R. Liandi, A. H. Cahyana, R. T. Yunarti and T. P. Wendari, *Ceram. Int.*, 2022, **48**, 20266–20274.
93 H. Veisi, T. Ozturk, B. Karmakar, T. Tamoradi and S. Hemmati, *Carbohydr. Polym.*, 2020, **235**, 115966.
94 M. Esmaeilpour, A. R. Sardarian and H. Firouzabadi, *J. Organomet. Chem.*, 2018, **873**, 22–34.
95 P. Chandane, J. Ladke, C. Jori, S. Deshmukh, S. Zinjarde, M. Chakankar and U. Jadhav, *J. Environ. Chem. Eng.*, 2019, **7**, 103083.
96 D. Hou, T. Yang, J. Tang and S. Li, *Phys. Chem. Chem. Phys.*, 2018, **20**, 8773–8789.
97 M. Aamir, M. Farooq, J. Ambreen, N. Ahmad, M. Iqbal, A. Haleem and M. Siddiq, *J. Environ. Chem. Eng.*, 2019, **7**, 103280.
98 M. Ariannezhad, D. Habibi and S. Heydari, *Polyhedron*, 2019, **160**, 170–179.
99 M. A. Ashraf, Z. Liu, W.-X. Peng and C. Gao, *Catal. Lett.*, 2020, **150**, 683–701.
100 M. Venkatesham, D. Ayodhya, A. Madhusudhan and G. Veerabhadram, *Int. J. Green Nanotechnol.*, 2012, **4**, 199–206.
101 A. Mazaheri and M. Bostanian, *Res. Chem. Intermed.*, 2020, **46**, 2327–2350.
102 K. Arora, D. Kumar, K. Burman, S. Agnihotri and B. Singh, *J. Saudi Chem. Soc.*, 2011, **15**, 161–165.
103 Y. Suneetha, B. N. Kumar, Y. Harinath, D. H. K. Reddy and K. Seshaiah, *Mikrochim. Acta*, 2012, **176**, 169–176.
104 R. K. Sharma, R. Gaur, M. Yadav, A. Goswami, R. Zbořil and M. B. Gawande, *Sci. Rep.*, 2018, **8**, 1901.
105 J. Kalidass, S. Anandan and T. Sivasankar, *Crystals*, 2023, **13**, 557.
106 K.-H. Tseng, H.-C. Ke and H.-C. Ku, *Nanomater. Nanotechnol.*, 2021, **11**, 18479804211035190.
107 T. Shamsi, A. Amoozadeh, S. M. Sajjadi and E. Tabrizian, *Appl. Organomet. Chem.*, 2017, **31**, e3636.
108 C. Cozic, L. Picton, M.-R. Garda, F. Marlhoux and D. Le Cerf, *Food Hydrocolloids*, 2009, **23**, 1930–1934.
109 A. Grein, B. C. da Silva, C. F. Wendel, C. A. Tischer, M. R. Sierakowski, A. B. D. Moura and I. C. Riegel-Vidotti, *Carbohydr. Polym.*, 2013, **92**, 312–320.
110 B. Niemczyk-Soczynska, A. Gradys and P. Sajkiewicz, *Polymers*, 2020, **12**, 2636.
111 P. J. Dyson and P. G. Jessop, *Catal. Sci. Technol.*, 2016, **6**, 3302–3316.
112 S. F. Hamzavi, S. Gerivani, S. Saeedi, K. Naghdipari and G. Shahverdizadeh, *Mol. Diversity*, 2020, **24**, 201–209.
113 M. Madasu, C. F. Hsia and M. H. Huang, *Nanoscale*, 2017, **9**, 6970–6974.
114 X. Xiong, Z. Tang, Z. Sun, X. Meng, S. Song and Z. Quan, *Appl. Organomet. Chem.*, 2018, **32**, e3946.
115 M. Rajabzadeh, R. Khalifeh, H. Eshghi and M. Sorouri, *Catal. Lett.*, 2019, **149**, 1125–1134.
116 F. Nemati, M. M. Heravi and A. Elhampour, *RSC Adv.*, 2015, **5**, 45775–45784.